Lab on a Chip

Cite this: DOI: 10.1039/c1lc20092e

www.rsc.org/loc

PAPER

Chromatographic behaviour of single cells in a microchannel with dynamic geometry†

Thomas Gerhardt,[a] Sangpil Woo[b] and Hongshen Ma*[acd]

Received 1st February 2011, Accepted 20th May 2011
DOI: 10.1039/c1lc20092e

We present the design of a microchannel with dynamic geometry that imparts different flow rates to different cells based on their physical properties. This dynamic microchannel is formed between a textured surface and a flexible membrane. As cells flow through the microchannel, the height of the channel oscillates causing periodic entrapment of the larger cells, and as a result, attenuating their velocity relative to the bulk liquid. The smaller cells are not slowed by the moving microstructure, and move synchronously with the bulk liquid. The ability of the dynamic microchannel to selectively attenuate the flow rate of eukaryotic cells is similar to a size-exclusion chromatography column, but with the opposite behavior. The speed of smaller substances is attenuated relative to the larger substances in traditional size-exclusion chromatography columns, whereas the speed of the larger substances that is attenuated in the dynamic microchannel. We verified this property by tracking the flow of single cells through the dynamic microchannel. L1210 mouse lymphoma cells (MLCs), peripheral blood mononuclear cells (PBMCs), and red blood cells (RBCs) were used as model cells. We showed that the flow rate of MLC is slowed by more than 50% compared to PBMCs and RBCs. We characterized the operation of the microchannel by measuring the velocity of each of the three cell types as a function of the pressures used to oscillate the membrane position, as well as the duty cycle of the oscillation.

Introduction

Size-exclusion chromatography is a classical technique for separating components of a mixture based on their ability to transit through a column of porous material.[1] This approach is used ubiquitously for the separation of molecules based on their hydrodynamic cross-section, enabling label-free separation with the ability to recover the target species. Size-exclusion chromatography has not been extended to the separation of eukaryotic cells because of the lack of column materials or structures that can impart sufficiently distinct flow velocities to different cell phenotypes to enable efficient separation. Microfabrication and microfluidics technologies present new capabilities to create complex microstructures and to precisely control the flow of minute volumes of liquid. Multi-layer soft lithography further enabled the ability to create moving microstructures that can function as micrometre-scale valves and pumps.[2] We exploit these technologies to develop a microchannel with dynamic structure capable of imparting different flow rates to cells with distinct physical properties. Such microchannels have the potential to perform separations in an analogous manner as size-exclusion chromatography column to separate cells based on their physical properties.

Our concept involves transporting cells through a microchannel formed between a textured surface and a flexible membrane shown in Fig. 1. The textured surface consists of an array of micrometre-scale pockets that temporarily entrap the larger cells in order to attenuate their flow velocity. The flexible membrane alters the height of the microchannel between an *open* state (Fig. 1B) and a *semi-closed* state (Fig. 1A and C) using externally applied pneumatic pressure. In the open state, all cells can traverse freely through the microchannel. In the semi-closed state, smaller cells can traverse freely through the microchannel, while larger cells are temporarily trapped by the microstructure. Rapid oscillation of the channel geometry between the open and semi-closed states enables serial entrapment of the larger cells resulting in consistent attenuation of their velocity thereby reducing their speed relative to smaller cells. The time fraction between the open and semi-closed states, known as the duty cycle, controls the ratio of the velocity of trapped *versus* free-flowing cells.

[a]*Department of Mechanical Engineering, University of British Columbia, 2054-6250 Applied Science Lane, Vancouver, BC, Canada V6T 1Z4. E-mail: hongma@mech.ubc.ca*
[b]*Department of Physics and Astronomy, University of British Columbia, Vancouver, Canada*
[c]*Department of Urologic Science, University of British Columbia, Vancouver, Canada*
[d]*Vancouver Prostate Centre, Vancouver General Hospital, Vancouver, Canada*
† Electronic supplementary information (ESI) available: See DOI: 10.1039/c1lc20092e

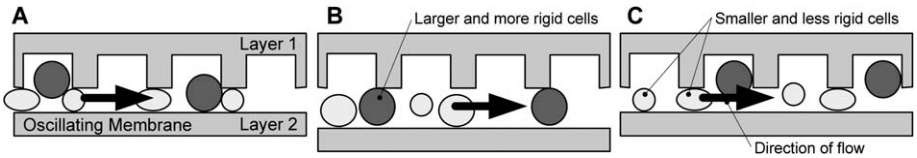

Fig. 1 Using a dynamic microchannel to selectively attenuate the velocity of larger and more rigid cells: (A) the semi-closed state holds the larger and more rigid cells in the traps, while smaller and less rigid cells pass freely through the microchannel. (B) The open state allows all cells to pass through the microchannel. (C) As the channel closes again, larger and more rigid cells slip into the next available trap while smaller and less rigid cells proceed unimpeded as before.

Existing microfluidic mechanisms for label-free cell-separation are based exclusively on the use of passive microstructures to impart different flow rates to different cell types. These mechanisms can be broadly classified into filtration and hydrodynamic manipulation. Filtration sieves a cell mixture using a set of small pores in order to trap the larger cells while eluting the smaller cells.[3–10] A significant problem with this approach is the tendency for the filter to clog when the larger cells become lodged in the pores ahead of smaller cells. The presence of the clogged pores alters the hydrodynamic resistance of the filter in an unpredictable manner, and as a result, compromises the selectivity of the filter. Furthermore, persistent (non-moving) contact between the cell membrane and the filter surface increases the potential for cells to be adsorbed onto the filter surface, which prevents the recovery of target cells after separation.

Hydrodynamic manipulation exploits the parabolic profile of fluid velocities near flow boundaries in laminar flow. When a cell mixture is propelled near such boundaries by geometrical constraint or by an external field, the hydrodynamic centers of different sized particles intercept different streamlines and therefore are imparted with different flow velocities. Examples of this technique include deterministic lateral displacement,[11,12] hydrodynamic filtration,[13] and field-flow fractionation.[14–16] Compared to traditional filtration, this approach is inherently less likely to clog because all components of the mixture are maintained in continuous flow. A key drawback of this technique, however, is that cells are separated based on size alone, but not rigidity, which is often a stronger parameter for discriminating different cell types and disease states.[17–23]

Our dynamic microstructure mechanism exhibits some of the advantages of both filtration and hydrodynamic manipulation. Similar to filtration, the dynamic microchannel mechanism has the potential to discriminate cells based on size and rigidity; while similar to hydrodynamic manipulation, the cells are maintained in continuous flow, which reduces the potential for surface adsorption. We now describe the detailed design of this dynamic microstructure and demonstrate its ability to impart differential flow velocities to cultured cancer cells and human blood cells.

Design

Oscillating membrane

The microchannel with dynamically adjustable height consists of a two-layer microstructure fabricated using multilayer soft lithography of polydimethylsiloxane (PDMS) silicone. Cross-sections of this device, in both open and semi-closed states, are shown in Fig. 2. The sample is infused into the flow channel, while the position of the membrane is controlled using the pressure applied to the control channel. A protruding center fin acts as a mechanical stop to flatten the control membrane and to prevent compression of the transiting cells. When the upward-deflected membrane comes into contact with the center fin, the single membrane surface is divided into two smaller surfaces of approximately half the original width. The membrane halves are stiffer than the original membrane and thus more easily resist further bending caused by the control channel pressure.[24] The presence of the center fin mechanical stop makes the operation of the membrane less sensitive to both the material stiffness of the membrane and the pressure applied in the control channel.

The control channel used to apply pressure to the membrane is a 25 μm thick rectangular cavity situated underneath, and completely overlapping, the flow channel. The control channel is formed by bonding the PDMS microstructure to a glass slide. In order to prevent the membrane from collapsing onto the glass slide during device fabrication and operation, 30 × 30 μm posts placed in a grid pattern with a 250 μm pitch are used to support the membrane in the control channel, as shown in Fig. 2. The posts are prevented from being attached to the glass slide by locally deactivating its PDMS-to-glass bond during fabrication.

Flow channel microstructures

In the open state, the microstructures are designed to allow all cells in the sample to transit. In the semi-closed state, the microstructures are designed to temporarily trap target cells but allow non-target cells to transit. The dimensions of this device are designed specifically to trap cultured cancer cells with a mean diameter of 10 μm, but allow the transit of peripheral blood mononuclear cells (PBMCs) with a mean diameter of 7.2 μm, as well as other smaller cells. Since single cells can transit through constrictions under modest compression, the height of the flow

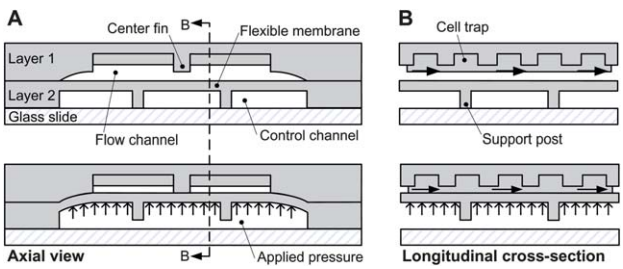

Fig. 2 The structure of the dynamic microchannel, in the open and the semi-closed states, is shown in (A) axial cross-section and (B) longitudinal cross-section.

channel in the semi-closed state is selected to be 7 μm, similar to the diameter of PBMCs. The height of the flow channel in the open state is selected to be 17 μm in order to accommodate occasional larger cells in the channel. Since the larger cells are only trapped in the microstructure temporarily, no additional mechanism is necessary to release the cells. The channel dimensions maybe further modified by adjusting the pressure applied to the control channel in the open and semi-closed states. The design and layout of this device is shown in Fig. 3. The prototype described here is designed with a 6000 μm long channel, which can be lengthened for future applications. The flow rate of cells in the flow channel is determined by the pressure applied across the inlet and outlet, as well as by the overall hydrodynamic resistance of the flow channel. Serpentine microchannels (Fig. 3B) are added to the inlet of the flow channel in order to increase the overall hydrodynamic resistance of the flow channel and to reduce the variation in the hydrodynamic resistance caused by membrane deflection.

Lateral cell motion

Preliminary experiments showed a tendency of the cells to travel longitudinally, as well as laterally toward the sides of the microchannel. This lateral cell motion is caused by the dynamics of membrane inflation, which begin at the center of the channel and propagate outwards toward the edge of the channel. As shown in Fig. 4A and B, membrane inflation deflects the target cells toward the edges of the channel where the channel height is lower and the cells have a greater chance of being damaged by the membrane deflection or being adsorbed onto the flow channel surfaces. This undesirable lateral movement is mitigated by an angled trap structure, as shown in Fig. 4C. The combination of the angled surfaces and viscous flow along the channel provides a force that pushes the target cells towards the center of the channel. During testing, these angled microstructures successfully restored the lateral position of the trapped cells towards the center of the channel.

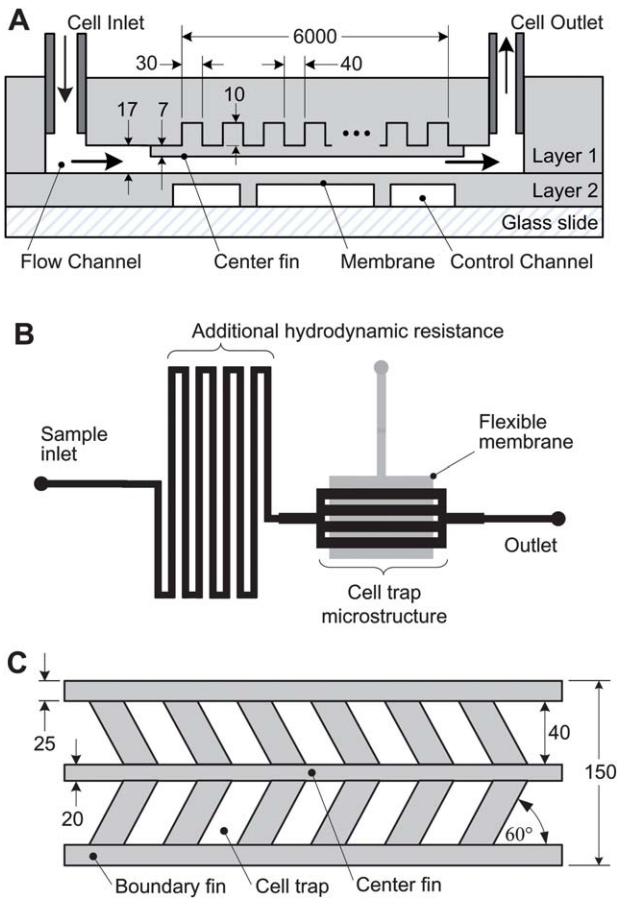

Fig. 3 Detailed design of the dynamic microchannel. (A) Cross-section of the dynamic microchannel. (B) Simplified layout of the dynamic microchannel device including the serpentine microchannel that provides additional hydrodynamic resistance to the inlet flow of the device. (C) Top-view of the detailed design of the angled cell-trap microstructure. All dimensions are in micrometres.

Materials and methods

Microfabrication

The flow layer microstructure was fabricated on a silicon wafer substrate by the Stanford Microfluidics Foundry (Stanford, CA, USA). Three photolithographically patterned layers consisting of SU-8 2010, 2015, and 2025 negative photoresists (Microchem, Newton, MA, USA) were deposited onto the wafer. Each photoresist layer was spun, exposed (after alignment), and then developed according to the manufacturer's instructions to produce the structure shown in Fig. 5. The control layer microstructure was fabricated using a single layer of SU-8 2025 by a similar process.

PDMS device fabrication and preparation

Silicon wafers containing the flow layer and control layer microstructures were initially replicated using a plastic molding technique.[25] PDMS devices were fabricated from plastic molds using multilayer soft-lithography of RTV 615 silicone (Momentive Performance Materials).[2] The control layer was spun onto a plastic copy of the silicon wafer at 1600 rpm, which produced a 40 μm thick layer. The flow layer was cast molded from its plastic master and diffusion bonded to the control layer. The bonded devices were cut and punched using a 0.5 mm diameter punch (Technical Innovations, Angleton, TX, USA) to create fluid ports. In preparation for bonding, both the PDMS devices and clean glass slides were activated using 40 s of air plasma (Harrick Plasma, Ithaca, NY, USA). Before bonding, however, a droplet of water was pipetted onto the membrane and the support post-areas of the device to deactivate the bond in these areas. After evaporation of the water droplet, the PDMS and glass pieces were pressed together to form a covalent bond on contact over the activated areas. The completed device was prepared for experiments by initially filling the control channels with de-ionized water using 200 mbar of pressure. Subsequently, the flow channels were infused with phosphate buffered saline containing 5% bovine serum albumin, and incubated for 30 minutes to prevent non-specific adsorption of the cells onto the surface of the PDMS.

Sample preparation

L1210 mouse lymphoma cells were grown in suspension culture using RPMI 1640 (Invitrogen) containing 10% fetal bovine

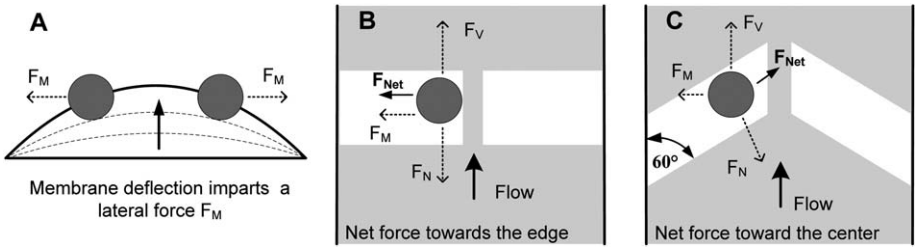

Fig. 4 (A) Inflation of the membrane pushes cells laterally towards the edge of the flow channel with the force F_M. (B) In cell traps arranged perpendicularly to the direction of the flow, there is no force to counteract F_M. (C) In angled cell traps, the viscous force from the flow, F_V, and the normal force from the trap walls, F_N, combine to push the cell towards the center of the channel.

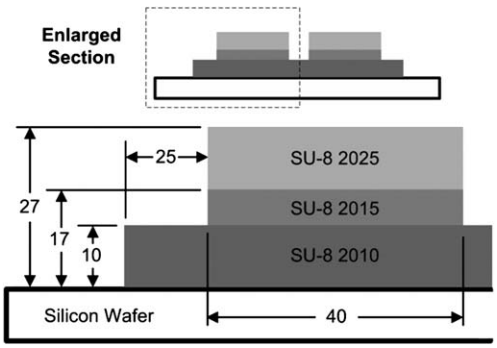

Fig. 5 Axial cross-section of the completed master mold for the flow layer fabricated using photolithography. The SU-8 2025 layer is not continuous along the length of the device and forms the temporary cell traps. All dimensions are in micrometres.

serum and 1% penicillin/streptomycin, at 37 °C in a 100% humidified atmosphere containing 5% CO_2. The cell suspension was diluted using phosphate buffered saline containing 5% bovine serum albumin. Cell viability was assessed using L3224 LIVE/DEAD Viability/Cytotoxicity Kit (Invitrogen) following the manufacturer's instructions. Peripheral blood mononuclear cells were prepared from whole blood collected from healthy volunteers following informed consent. Whole blood was drawn into 6 mL sodium heparin containing tubes. Peripheral blood mononuclear cells were obtained using Histopaque 1077 (Sigma-Aldrich) according to manufacturer's instructions, and then re-suspended at a concentration of 10×10^6 cells per mL in AIM 5 media (Invitrogen). Red blood cells were purified from whole blood and used within 48 hours of donation. Before testing, each of the three cell types was re-suspended to a concentration of 7×10^8 cells per mL.

Experimental apparatus

Fluids infused into the microfluidics device were supplied from 15 mL sealed conical tubes (Fisher Scientific) with custom fabricated caps that enable the tubes to act as pressurized reservoirs. The liquid connection between the reservoirs and the device was made using 0.5 mm ID flexible Tygon tubing (Cole-Parmer). The device-to-tube interface was created using 19 mm long 23 gauge stainless steel tubing (New England Small Tube, Litchfield, NH, USA) that forms a stretch seal between the PDMS device and the Tygon tubing. A multi-channel pressure control system (Fluigent MFCS-4C, France) was used to pressurize the reservoirs connected to the flow channel. A custom-made pressure control system was used to pressurize the reservoirs connected to the control channel to deflect the membrane. Pressure applied to the control channel could be turned on and off automatically using solenoid valves controlled by a MSP430 microprocessor (Texas Instruments) and custom-developed PC software.

Data analysis

Videos of the cell motion inside the microchannel were acquired using a Nikon Ti-U inverted microscope and a Nikon DS-2MBW CCD camera. The displacement of individual cells was measured using frame-by-frame tracking in the captured videos. The net velocity of each cell was determined using the slope of a linear fit to the displacement data. Cell diameters were measured in suspension using the Nikon NIS-Elements image capture software supplied with the CCD camera.

Results and discussion

We studied the chromatographic properties of the dynamic microchannel using red blood cells (RBCs), peripheral blood mononuclear cells (PBMCs), and L1210 mouse lymphoma cells (MLCs). RBCs are highly deformable, discoid-shaped cells with an 8 μm diameter and a 2 μm thickness. Because the dimensions of RBCs are small relative to the length scale of the microstructures, these cells essentially follow the flow of the bulk liquid. PBMCs primarily consist of lymphocytes and have a measured mean diameter of 7.2 μm with a standard deviation of 0.6 μm. MLCs were grown from an immortalized cell line and used in experiments between 4 and 6 days after passage. During this period, these cells had a mean diameter of 10.0 μm with a standard deviation of 1.4 μm. MLCs were chosen because their size and shape are somewhat similar to PBMCs, but their rigidity is likely to be significantly greater because of their enlarged nucleus.

The flow properties of each of the three cell types in the dynamic microchannel were tracked by following the displacement of individual cells over a fixed 2500 μm section of the microchannel. Representative cell displacement data graphs are shown in Fig. 6A. The sample fluid was infused into the microchannel with a pressure of 20 mbar, while the membrane inflation pressure was oscillated between 100 mbar for the open state and 230 mbar for the semi-closed state. The membrane oscillation had a period of 6 seconds and a duty cycle of 50%. The timing of

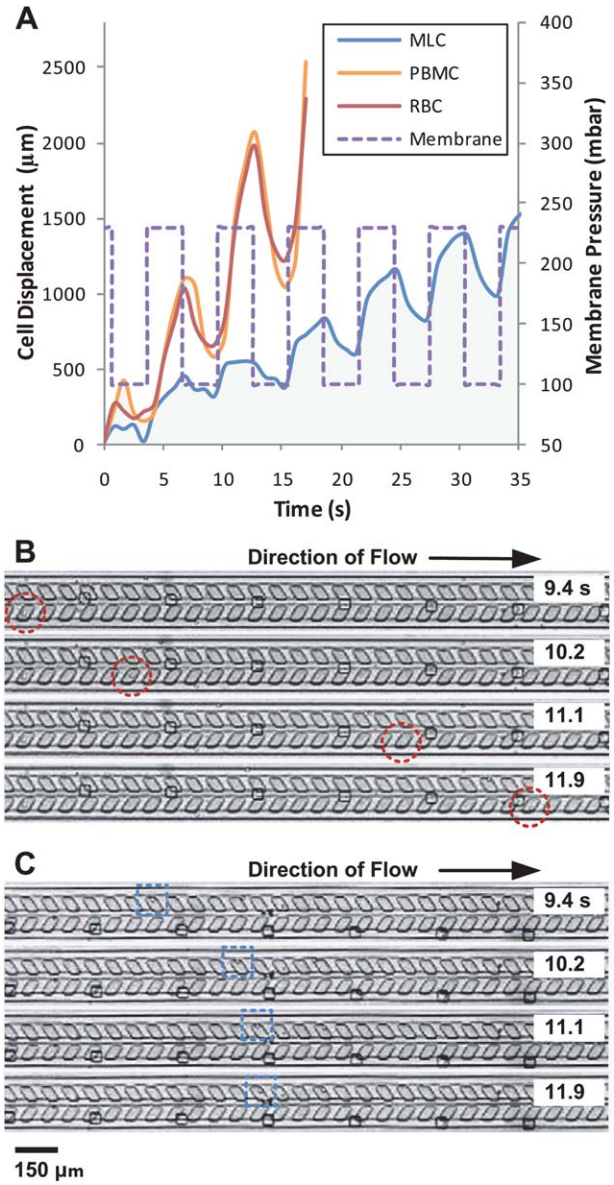

Fig. 6 (A) Displacement *versus* time graph of single MLCs, PBMCs, and RBCs tracked over a 2500 µm section of the dynamic microchannel shown with the applied oscillatory pressure signal. (B) Images from the semi-closed state where RBCs move with little impedance. (C) Images from the semi-closed state where MLCs are trapped by the microstructure.

each data graph was adjusted to match the phase of the membrane oscillations in Fig. 6A. Cell viability was checked repeatedly along the length of the microchannel using the fluorescence signal produced by the L3224 LIVE/DEAD viability assay (Invitrogen). No changes in cell viability were observed, which is consistent with previous observations of eukaryotic cells compressed by PDMS membrane microvalves.[2]

To understand the process by which the dynamic microchannel selectively imparts different flow velocities to larger cells, consider the displacement of the MLC in Fig. 6A at the transition point between the open state and the semi-closed state. The inflation of the membrane constricts the flow channel and expels liquid that accelerates the MLC downstream. This downstream bias is caused by the serpentine inlet channel shown in Fig. 3B that presents a large hydrodynamic resistance in the upstream direction. As MLCs are temporarily captured by the cell traps, their flow rate is slowed dramatically, eventually coming to a complete stop inside the cell traps. Fig. 6C shows selected images from a video tracking the flow of a single MLC during this period. The bulk liquid is not slowed by the presence of the traps and separates from the MLC. When the membrane is deflated and the flow channel transitions back to the open state, liquid is temporarily drawn backwards in the channel before constant forward flow is restored. This backward flow is non-selective and propels the MLC and the bulk liquid at approximately the same velocity. The asymmetrical flow behavior combined with the periodic inflation and deflation of the membrane enables the dynamic microchannel to ratchet the MLCs backwards against the motion of the bulk liquid. A movie showing the flow of MLCs can be seen in Video S1†.

RBCs and PBMCs are not trapped by the channel microstructure, and as a result, follow the flow of the bulk liquid. Fig. 6B shows images from a video tracking the flow of a single RBC at the transition between the open state and the semi-closed state. These images are synchronized to Fig. 6A using the displacement of the membrane. Over the length of the observed section of the microchannel, the displacement of RBCs shown in Fig. 6A is the superposition of a constant forward flow and an oscillatory flow caused by the membrane oscillation. A movie showing the flow of RBC can be seen in Video S2†. Interestingly, the displacement of PBMCs follows RBCs almost exactly even though PBMCs are required to undergo a slight compression by the membrane. This result suggests that the dynamic microchannel has the potential to discriminate the cell suspension into a population temporarily trapped by the microstructures and a population unaffected by the microstructures. The oscillatory flow of the RBCs and PBMCs increases in amplitude downstream in the channel due to the presence of the large hydrodynamic resistance in the upstream direction created by the serpentine inlet channels. In future implementations, the transient oscillatory flow of these cells and of the bulk liquid can be dampened using dynamic microchannels containing multiple membrane sections that are inflated out-of-phase with one another.

The distinct transient flow characteristics of MLCs compared to PBMCs and RBCs result in different net velocities that will enable cell separation over a sufficiently long stretch of the dynamic microchannel. The net velocity of each cell type in the channel can be estimated using a linear fit of the displacement data graphs. Key operating parameters that control the net cell velocity in this device are the pressure applied to the membrane in the semi-closed state, as well as the duty cycle of the membrane oscillation. If the membrane pressure is too small during the semi-closed state, the channel is insufficiently constricted to significantly attenuate the velocity of the target cells. If the membrane pressure is too large, the target cells may be prevented from entering the microchannel.

The net velocities of MLCs, PBMCs, and RBCs were measured as a function of the membrane pressure in the semi-closed state. For these experiments, the open state pressure was fixed at 100 mbar and the membrane duty cycle at 50%. The results are plotted in Fig. 7A, where each data point is the

average net flow velocity of 8 individual cells, while the error bars show the standard deviation. As expected, the average velocities of PBMCs and RBCs are nearly identical and are unaffected by the value of the membrane pressure. The average velocity of the MLCs is reduced relative to PBMCs and RBCs, with a distinct transition near 200 mbar. Below 200 mbar, the average velocity of MLCs is approximately 0.7 times the velocities of PBMCs and RBCs. Above 200 mbar, this ratio is approximately 0.4. This bimodal behavior can be explained from the MLC displacement *versus* time plots shown in Fig. 7B for below and above the 200 mbar transition. When the membrane is inflated with less than 200 mbar of pressure, the cell traps only slow the velocity of MLCs, but cannot completely stop them during the semi-closed state. In contrast, above 200 mbar, the MLCs come to a complete stop during each cycle of membrane inflation. Fig. 7A also shows a slight increase in the average velocity of MLCs at the 250 mbar data point. This trend is caused by the membrane being sufficiently over-inflated to prevent some of the larger MLCs from entering the dynamic microchannel, in which case the microchannel is selective for smaller cells that tend to exhibit greater net velocities.

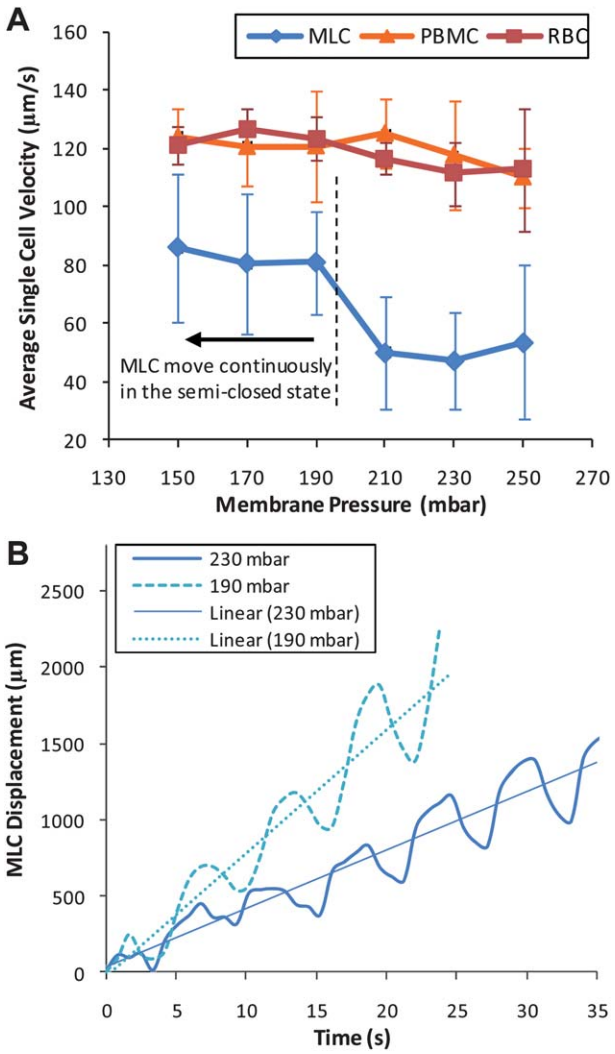

Fig. 7 (A) The average forward velocity of all three cell types as a function of pressure. Data points are the mean values of 8 cells. Error bars indicate standard deviation. (B) The displacement *versus* time graph of MLCs at membrane pressures above and below the transition in (A).

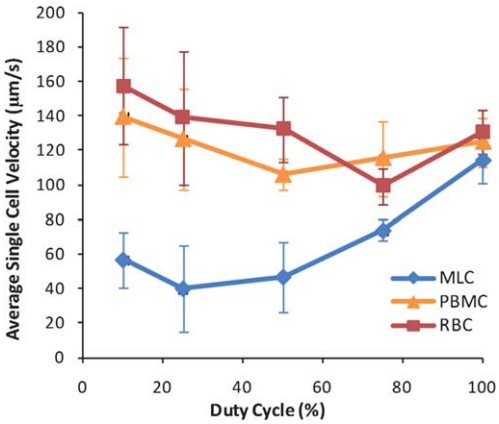

Fig. 8 The average forward velocity of each of the three cell types as a function of duty cycle. Data points are the mean values of 8 cells. Error bars indicate standard deviation.

The duty cycle of the dynamic microchannel is defined as the ratio between the duration of the open state and the period of the total oscillation. Fig. 8 shows the duty cycle dependence of the average velocity of each of the three cell types. These measurements were taken with open and semi-closed state membrane pressures set at 100 and 230 mbar respectively. As expected, the average velocity of MLCs shows a decreasing trend as the duty cycle is reduced from 100%, whereas the net flow rates of PBMCs and RBCs are nearly identical to each other and show little dependence on duty cycle. The average velocity of PBMCs and RBCs shows a general tendency to increase at lower frequencies. This trend likely results from reduced interactions between these cells and the surfaces of the dynamic microchannel. Below a 40% duty cycle, the average velocity of MLCs also begins to increase with decreasing duty cycle. Similar to over-pressurizing the membrane, this property is caused by the motion of the membrane that excludes some of the larger MLCs because the length of time of the open state is insufficient for these cells to enter the microchannel.

Conclusion

We conclude that a microchannel with dynamic geometry provides a new method to selective attenuate the flow rate of eukaryotic cells based on their physical properties. We demonstrated that larger cells can be serially retained as they traverse through the microstructures, which reduces their velocity relative to the velocity of smaller cells. This behavior is exactly the opposite of traditional size-exclusion chromatography where larger substances traverse the column at a greater speed than smaller substances. Consequently, the dynamic microstructure mechanism is particularly well suited for concentrating and enriching rare cells that are larger and/or more rigid than the background cells of a mixture. Future studies will focus on the separation and enrichment of cells from mixtures, the mechanisms of zone broadening in long microchannels, and methods to reduce the amplitude of the oscillatory transient flow.

Acknowledgements

The authors are grateful for technical contributions from members of the Multi-scale Design Laboratory at UBC. The authors would like to thank Elena Polishchuk, Dana Kyluik, and Mark Scott for providing materials used in this study. They would also like to thank Maria Gyongyossy-Issa, George M. Homsy, and Boris Stoeber for helpful suggestions. This work was supported in part by the Natural Science and Engineering Research Council of Canada and the PC-TRIADD Centre for Excellence in Research and Commercialization at the Vancouver Prostate Centre.

References

1 E. Heftmann, *Chromatography: Fundamentals and Applications of Chromatography and Related Differential Migration Methods*, Elsevier, Amsterdam, New York, 1992.
2 M. A. Unger, H. P. Chou, T. Thorsen, A. Scherer and S. R. Quake, *Science*, 2000, **288**, 113–116.
3 X. Chen, D. F. Cui, C. C. Liu and H. Li, *Sens. Actuators, B*, 2008, **130**, 216–221.
4 H. M. Ji, V. Samper, Y. Chen, C. K. Heng, T. M. Lim and L. Yobas, *Biomed. Microdevices*, 2008, **10**, 251–257.
5 H. Mohamed, M. Murray, J. N. Turner and M. Caggana, *J. Chromatogr., A*, 2009, **1216**, 8289–8295.
6 S. Murthy, P. Sethu, G. Vunjak-Novakovic, M. Toner and M. Radisic, *Biomed. Microdevices*, 2006, **8**, 231–237.
7 S. H. Seal, *Cancer*, 1964, **17**, 637–642.
8 S. Tan, L. Yobas, G. Lee, C. Ong and C. Lim, *Biomed. Microdevices*, 2009, **11**, 883–892.
9 V. VanDelinder and A. Groisman, *Anal. Chem.*, 2007, **79**, 2023–2030.
10 G. Vona, A. Sabile, M. Louha, V. Sitruk, S. Romana, K. Schutze, F. Capron, D. Franco, M. Pazzagli, M. Vekemans, B. Lacour, C. Brechot and P. Paterlini-Brechot, *Am. J. Pathol.*, 2000, **156**, 57–63.
11 J. A. Davis, D. W. Inglis, K. J. Morton, D. A. Lawrence, L. R. Huang, S. Y. Chou, J. C. Sturm and R. H. Austin, *Proc. Natl. Acad. Sci. U. S. A.*, 2006, **103**, 14779–14784.
12 L. R. Huang, E. C. Cox, R. H. Austin and J. C. Sturm, *Science*, 2004, **304**, 987–990.
13 M. Yamada and M. Nakashima, *Anal. Chem.*, 2004, **76**, 33–36.
14 M. A. Benincasa, L. R. Moore, P. S. Williams, E. Poptic, F. Carpino and M. Zborowski, *Anal. Chem.*, 2005, **77**, 5294–5301.
15 J. C. Giddings, *Science*, 1993, **260**, 1456–1465.
16 X. B. Wang, J. Yang, Y. Huang, J. Vykoukal, F. F. Becker and P. R. C. Gascoyne, *Anal. Chem.*, 2000, **72**, 832–839.
17 S. Chien and K. L. P. Sung, *Biophys. J.*, 1984, **46**, 383–386.
18 S. E. Cross, Y. S. Jin, J. Rao and J. K. Gimzewski, *Nat. Nanotechnol.*, 2007, **2**, 780–783.
19 R. M. Hochmuth, *J. Biomech.*, 2000, **33**, 15–22.
20 W. R. Jones, H. P. Ting-Beall, G. M. Lee, S. S. Kelley, R. M. Hochmuth and F. Guilak, *J. Biomech.*, 1999, **32**, 119–127.
21 G. Y. H. Lee and C. T. Lim, *Trends Biotechnol.*, 2007, **25**, 111–118.
22 M. J. Rosenbluth, W. A. Lam and D. A. Fletcher, *Biophys. J.*, 2006, **90**, 2994–3003.
23 K. J. Van Vliet, G. Bao and S. Suresh, *Acta Mater.*, 2003, **51**, 5881–5905.
24 V. Studer, G. Hang, A. Pandolfi, M. Ortiz, W. F. Anderson and S. R. Quake, *J. Appl. Phys.*, 2004, **95**, 393–398.
25 S. P. Desai, D. M. Freeman and J. Voldman, *Lab Chip*, 2009, **9**, 1631–1637.